Identifying distinct thermal components of a creek

David A. Boughton,[1,2] Christine Hatch,[3] and Ethan Mora[4]

Received 5 December 2011; revised 11 June 2012; accepted 16 July 2012; published 6 September 2012.

[1] Statistical and heat budget methods for analyzing temperature dynamics of creeks are limited by the ability to resolve thermal processes and fine-grained thermal structures, respectively. Here we describe a hybrid method that identifies distinct thermal components in a stream's heat budget using only temperature data and an algorithm that employs mutual information to "unmix" signals in the temperature data. Spatial resolution is limited only by the number of temperature-logging sensors, which can be quite high for distributed-temperature sensors. Process resolution is at the level of thermal components, defined as distinct collections of heat flux elements sharing coordinated (nonindependent) dynamics. Inference can be used to relate thermal components to meteorological forcing and structural heterogeneity in the fluvial system and to suggest novel hypotheses for further testing with targeted heat budget studies. Applying the method to a small, arid-land creek produced two novel hypotheses: (1) lateral conduction of heat from adjacent dry land (bed, terraces) appeared to cause a substantial heating of the stream, augmented by off-channel flow paths, and (2) riparian vegetation was associated with a subtraction of heat from the stream at a rate proportionate to solar insolation, exceeding the maximum decoupling effect of shade by at least 2°C at midday, and suggesting upwelling heat flux from water to tree canopy proportional to sunlight. The method appears useful for generating new hypotheses, for selecting informative sites for detailed heat budgets, for determining the dimensionality of heat budgets in natural streams, and more broadly for associating thermal components to fluvial structure and processes.

Citation: Boughton, D. A., C. Hatch, and E. Mora (2012), Identifying distinct thermal components of a creek, *Water Resour. Res.*, *48*, W09506, doi:10.1029/2011WR011713.

1. Introduction

[2] Freshwater creeks are a widespread habitat where temperature plays an important role in structuring and sustaining aquatic biodiversity. Recent reviews emphasize that freshwater thermal regimes are coupled to climate, but with substantial spatial and temporal heterogeneity linked to local channel conditions that insulate and buffer thermal dynamics [*Caissie*, 2006; *Poole and Berman*, 2001; *Webb et al.*, 2008]. This thermal heterogeneity creates habitat features that are actively exploited by fish and other aquatic organisms [*Ebersole et al.*, 2001, 2003; *Isaak and Hubert*, 2004; *Torgersen et al.*, 1999].

[3] As climate change accelerates over the coming decades, resource managers will need to learn to characterize, manage, and even establish thermal habitat features in freshwater systems [*Ormerod*, 2009; *Wilby et al.*, 2010], implying a need for process-based frameworks that link channel organization and thermal condition. Two analytical frameworks commonly used for this purpose are statistical methods and heat budget methods.

1.1. Statistical Methods

[4] Statistical methods estimate the responsiveness of entire creeks and rivers to climate patterns, using temperature time series and regression models [*Eaton and Scheller*, 1996; *Isaak et al.*, 2010; *Mantua et al.*, 2010; *Mohseni et al.*, 2003; *Morrill et al.*, 2005]. Statistical methods can be effective for estimating mean stream temperature at temporal resolutions of a week or coarser, because weekly thermal budgets of streams can be approximated by equilibrium models [*Bogan et al.*, 2003; *Mohseni et al.*, 1998]. Weekly water temperature tends to track nearby air temperatures, but the tracking is not one to one: the responsiveness of streams to air temperature varies substantially across streams (e.g., 0.3°C water/°C air, to 1.09°C water/°C air in *Morrill et al.* [2005]), presumably due to quantitative differences in radiation, conduction, convection and advection processes in the riparian corridor [*Benyahya et al.*, 2012]. These differences imply diversity in the internal structure of the riparian system [*Poole and Berman*, 2001]. Each stream requires its own data and regression, sometimes allowing for limited process inference via covariate analysis (e.g., streamflow in *Caissie et al.* [2001]).

[1]Fisheries Ecology Division, Southwest Fisheries Science Center, National Marine Fisheries Service, NOAA, Santa Cruz, California, USA.
[2]Formerly at Department of Geological Sciences, University of Nevada, Reno, Nevada, USA.
[3]Geosciences Department, University of Massachusetts, Amherst, Massachusetts, USA.
[4]Joint Institute of Marine Observations, University of California, Santa Cruz, California, USA.

Corresponding author: D. A. Boughton, Fisheries Ecology Division, Southwest Fisheries Science Center, National Marine Fisheries Service, NOAA, 110 Shaffer Rd., Santa Cruz, CA 95060, USA.

[5] Limitations of the statistical approach are the omission of fine-scale thermal features, such as cold patches that are used by salmonids and other cold-water fishes [*Ebersole et al.*, 2001, 2003; *Matthews and Berg*, 1997; *Matthews et al.*, 1994; *Torgersen et al.*, 1999]; prediction error on the order of ±2°C [*Caissie et al.*, 2001; *Mohseni et al.*, 1998; *Morrill et al.*, 2005], which is large enough to have ambiguous implications for many species over broad areas; and poor ability to resolve the underlying physical processes.

1.2. Heat Budget Methods

[6] Heat budget methods enumerate and quantify the various physical pathways by which heat enters and exits a stream reach and thus can provide a great deal of insight about underlying processes [*Benyahya et al.*, 2012; *Boyd and Kasper*, 2003; *Brown*, 1969; *Evans et al.*, 1998; *Hebert et al.*, 2011; *Webb and Zhang*, 1997]. These physical pathways, or heat flux elements, are numerous and often vary over short temporal and spatial scales [*Boyd and Kasper*, 2003]. Accordingly, heat budget methods generally require detailed measurements of many individual flux elements. For example, *Evans et al.* [1998] estimated 20 different heat flux elements in the thermal budget of River Blithe, Staffordshire, UK. They found the river's heat budget to be dominated by a subset of 5 heat flux elements: net short-wave radiation, net long-wave radiation, evaporation, conduction with the riverbed, and sensible heat transfer. In a regional study of heat budgets, *Webb and Zhang* [1997] also found subsets of elements dominating, but these varied spatially and seasonally, suggesting a key role for process heterogeneity in the thermal budgets of stream systems [*Johnson*, 2004].

[7] Understanding process heterogeneity is a challenge. It is often impractical to estimate some heat flux elements at more than one or a few points in a channel. For such elements, constructing the overall heat budget requires an assumption that point estimates accurately represent mean flux over a broader area, implicitly assuming spatial homogeneity. For example, *Brown* [1969] assumed that net heat flux across the water-streambed interface could be estimated from a single point measurement for each of three streams in Oregon. *Benyahya et al.* [2012] measured short- and long-wave energy exchange between a stream and its tree canopy at one point, assumed to be representative.

[8] A related challenge is that different heat flux elements are unlikely to vary independently of one another in space and time—rather one expects them to be jointly structured by a riparian system of streamflow, riparian vegetation, bed forms, and groundwater flux [*Poole and Berman*, 2001]. Understanding process heterogeneity at the level of the riparian system, by measuring numerous nonindependent heat flux elements, some of which are difficult to measure at even a single point, is often impractical. For example, riparian vegetation influences local wind speeds [*Bogan et al.*, 2004], affecting both evaporative and convective heat transfer at the air-water interface. It shades the channel, intercepting substantial short-wave solar radiation [*Benyahya et al.*, 2012; *Hannah et al.*, 2008; *Webb and Zhang*, 2004]; shading varies seasonally, with leafing-out and senescence [*Benyahya et al.*, 2012]; and diurnally, as a function of sun angle [*Leach and Moore*, 2010]; and vegetation produces fine-grained spatial variation in shading and wind, so that associated heat fluxes cannot be reliably characterized by one or a few sensors [*Benyahya et al.*, 2012]. More subtly, vegetation heats up in the sun and emits long-wave radiation in a highly dynamic way [*Benyahya et al.*, 2012]. Heat movement in bed forms and associated patterns of subsurface flow can also be intricately structured [*Arrigoni et al.*, 2008; *Burkholder et al.*, 2008] and involve nonindependent heat flux elements [*Story et al.*, 2003].

1.3. A Hybrid Method

[9] For clarity we refer to the coordinated systems of heat flux elements described above as heat flux components. We suggest that a useful avenue of research is the characterization of heat flux components and their associations with patterns of streamflow, riparian vegetation, bed forms, and subsurface water movement. This view is motivated by the perspective that heat budgets are interesting not because they quantify each heat flux element, but because they show how stream systems self-organize heat flux elements in space and time. This self-organization means that strategies for managing thermal habitat will be more self-perpetuating if they address fluvial processes and related heat flux components, rather than the individual heat flux elements [*Poff et al.*, 2010; *Thorp et al.*, 2006; *Wilby et al.*, 2010]. But this perspective requires a method for identifying the components and relating them to fluvial processes.

[10] Here we describe a distinct-components method that combines features of the statistical and heat budget approaches. The method identifies distinct components of a creek's heat budget from dense temperature data, using a machine-learning technique known as least-dependent components analysis (LDCA) [*Stogbauer et al.*, 2004]. LDCA is a form of blind source separation, a family of methods for unmixing blended signals. The guiding metaphor for blind source separation is a noisy cocktail party, in which an array of microphones records different mixtures of the same set of conversations. The goal of blind source separation is to unmix the noisy party chatter back to a set of individual conversations, using no additional outside information. Here we unmix stream temperature data, interpreting the result as a set of distinct heat flux components, to which formal or informal inference can then be applied to better understand process heterogeneity. The method of distinct components has three ingredients:

[11] 1. A study area providing informative contrasts, defined here as stream channel(s) with structural heterogeneity that might be associated with thermal heterogeneity. A fundamental assumption is that the structural heterogeneity reflects different fluvial processes affecting heat flux, and can be interpreted as such—normally different types of vegetation, streamflows, bed forms, subsurface flow patterns, and/or microclimates.

[12] 2. A dense data set of stream temperatures from the study area. Dense as used here means 10 s to 1000 s of spatial positions and 100 s to 10000 s of points in time. A distributed temperature sensor (DTS) can be used to collect dense temperature data with resolutions down to 1 m and 1 min and extents of up to 10 km for days to months. A more flexible method is to deploy 10 s to 1000 s of inexpensive temperature loggers across entire stream networks; spatial resolution is limited by the number of loggers relative to total channel length.

[13] 3. Least-dependent components analysis [*Stogbauer et al.*, 2004], which unmixes the dense temperature data into a small number of maximally independent (or least-dependent)

time series, interpreted as distinct thermal components. The time evolution of thermal components can be compared to one another or analyzed via standard covariate analysis. The spatial profile of thermal components can be examined for relationships with structural heterogeneity of the channel, perhaps suggesting new insights or novel hypotheses that can be tested with conventional heat budget methods.

[14] Distinct components can be thought of as a parsimonious set of unobserved, maximally independent covariates implied by the data set. Unlike standard statistical methods, the components do not require observable covariates to be identified, though observable covariates may be useful for providing insights about the components—including the insight that some components do not have observable covariates. In addition, though the method does not identify heat flux elements, it does produce components with finer spatial and temporal resolution than the elements of a typical heat budget method. It can thus be used to provide context for more detailed heat budget methods; to assist in the siting of representative spatial points for heat budget methods, or to generate novel hypotheses that can be more rigorously tested using heat budget methods. In the remainder of this paper we outline the theoretical basis for the method and than illustrate its application to a small intermittent creek in central California, where cold-water conditions (<18°C) persist in the warm season, despite dwindling flows (<0.05 $m^3 s^{-1}$) and surrounding air temperatures that routinely exceed 35°C.

2. Method of Distinct Components

2.1. Reorganizing the Heat Flux Equation

[15] The basic equation for temperature evolution in a stream segment is

$$T_{t+1} = T_t + \Delta t \frac{k}{V_{t+1}}(Q_a + Q_b + Q_c + \ldots) \quad (1)$$

[*Boyd and Kasper*, 2003; *Brown*, 1969; *Webb and Zhang*, 1997], where T_t is mean temperature of the segment (°C) at time step t, and Δt is the time interval between steps (h). The heat flux elements Q_a, Q_b, … are mean rates of energy transfer (W per segment per element) due to individual physical mechanisms a, b, … over the interval Δt. The summed flux (net energy flux) is converted to temperature changes proportional to k, a factor converting seconds to hours ($s\ h^{-1}$) divided by the specific heat of water ($J\ kg^{-1}\ ^\circ\ C^{-1}$) and the mass density of water ($kg\ m^{-3}$), both effectively constant at the temperatures and pressures involved. Temperature changes are inversely proportional to the mean volume of water V_{t+1} (m^3) in the segment at the end of the time step. Considering multiple time steps at multiple adjacent locations, the time series for each location i can be represented as

$$T_{[t,i]} = T_{[0,i]} + \Delta t \sum_{m=1}^{M} \sum_{j=1}^{t} \left(\frac{k}{V_{[j,i]}} Q_{[j,i,m]} \right) \quad (2)$$

because heat fluxes are additive. The equation is arranged so that the term in parentheses is a component of temperature change at each time step due to heat flux m and volume $V_{[j,i]}$. For clarity, summarize this quantity as $q_{[j,i,m]}$, a component of temperature change, which implies a corresponding additive component of the temperature time series,

$$C_{[t,i,m]} = C_{[0,i,m]} + \Delta t \sum_{j=1}^{t} q_{[j,i,m]} \text{ where } T_{[t,i]} = \sum_{m} C_{[t,i,m]} \text{ for all } t. \quad (3)$$

Note that $C_{[\bullet,i,m]}$ (where • means all j) is a time series of temperature components (units: °C) due to heat flux m, and $q_{[\bullet,i,m]}$ is a time series of the m-specific heating rates (units: $^\circ C\ h^{-1}$).

2.2. Identifying the Least-Dependent Components

[16] Because heat fluxes are additive, the structure of (3) is flexible enough to regard m as indexing either heat flux elements or heat flux components (fractional combinations of elements with coordinated dynamics). Here we define a component-wise heat budget as a partitioning into a set of components m that minimize dependence of the $C_{[\bullet,i,m]}$ between different m. By partitioning dense temperature data into least-dependent components, the method (implicitly) maximizes codependence of (unspecified) heat flux elements within each component. This follows from the properties of information theory underlying LDCA: the method does not lose information, it merely redistributes it among the rows of the data matrix so as to minimize dependence among rows.

[17] More specifically, let $\mathbf{T}_{[i,t]}$ be a dense temperature matrix, and identify the square matrix $\mathbf{R}$ so that in

$$\mathbf{C} = \mathbf{RT}, \quad (4)$$

the rows of $\mathbf{C}$, corresponding to temperature components, are maximally independent. The LDCA algorithm uses mutual information, derived from information theory [*Kraskov et al.*, 2004; *Shannon*, 1948], as its measure of dependence. It is the expected shared information content of two random variables, and can be used to consistently compare dependencies between any pair of arbitrarily complex, multivariate time series. Information-theoretic properties of entropy and mutual information simplify the problem of finding $\mathbf{R}$ (unmixing the signals) into a tractable problem of systematically searching a space of rotation matrices (the MILCA algorithm of *Stogbauer et al.* [2004]). In our procedure we use the time delay embedding version of the MILCA algorithm, which accounts for time structure in $\mathbf{T}$ (see step 3 of Table 1, which outlines the entire procedure).

[18] Simple application of the MILCA algorithm to dense temperature data is underdetermined, because mutual information (MI) is invariant to any one-to-one transformations of the rows of $\mathbf{C}$ or $\mathbf{T}$ [*Kraskov et al.*, 2004]; this includes all smooth monotonic transformations of the data. Underdetermination is partly fixed by equation (3), which implies a constraint in the minimization problem: the sum of $C_{[t,i,m]}$ across m must be constant across rotations. The constraint is respected by applying MILCA to square root transformed temperature data, then squaring the resulting components (which conserves summed $C_{[t,i,m]}$ via the Pythagorean theorem). This fixes underdetermination down to location and scale, which are in turn fixed by centering the components and standardizing the mean components (across all spatial points) to sum to the mean temperature series (see steps 3

Table 1. Steps to Identify Distinct Components of Stream Temperature From a Dense Data Set **T**

Step	Action
1	Apply the MI-based clustering algorithm [*Kraskov et al.*, 2005] to the temperature matrix **T**.
2	Choose a number of groups, compute the mean time series for each group, and assemble into matrix $\mathbf{T_2}$ (rows = groups, columns = times)
3	Apply the time delay MILCA algorithm [*Stogbauer et al.*, 2004] to scalar square-root-transformed $\mathbf{T_2}$. Square each entry of the output matrix and center each row (mean = 0) to obtain $\mathbf{C_{unscaled}}$.
4	Compute the row vector $\mathbf{T_{mean}}$, the mean time series for **T** across all segments.
5	Use least squares to rescale the rows of $\mathbf{C_{unscaled}}$ to sum to $\mathbf{T_{mean}}$, to obtain $\mathbf{C_{mean}}$ (temperature components of the mean time series).
6	Sort the components (rows) of $\mathbf{C_{mean}}$ by amplitude or σ, and discard the trivial (nearly flat) components. If no nearly flat components, increase the number of groups and return to step 2.
7	Rescale remaining rows of $\mathbf{C_{mean}}$ so each has zero mean and unit variance, to obtain $\mathbf{C_z}$.
8	For each spatial segment (column) of **T**, use $\mathbf{C_z}$ and least squares (linear regression) to estimate constant, Gaussian, and responsiveness terms to obtain $\mathbf{R_2}$ (rows = segments, columns = terms). If Gaussian terms are large, decrease number of trivial components and return to step 6.
9	Multiply column m of $\mathbf{R_2}$ by corresponding row m of $\mathbf{C_z}$ to obtain $\mathbf{C_m}$ (temperature component m, as anomalies centered on zero).
10	Compute lag-1 differences of $\mathbf{C_m}$ and divide by scalar Δt to obtain $\mathbf{q_m}$ (heating rates for component m at each time step.

through 5 in Table 1). The components then have the interpretation of anomalies from the grand mean temperature.

2.3. Eliminating Trivial Components

[19] After LDCA, **C** has the same number of rows as **T**, sorted so that rows 1 and 2 are least dependent, rows 2 and 3 are the next least dependent, and so on. Generally the number of distinct components will tend to be much smaller than the number of rows (sites) in **T**, meaning that many rows of **C** will be very similar to one another, usually by being either very small anomalies (nearly flat components) or random noise. We call these trivial components. Our procedure replaces the trivial components with two standard components, an assumed flat line and Gaussian noise (steps 6–8 in Table 1). A new matrix $\mathbf{R_2}$ (no longer square) now shows the loadings ("responsiveness") of each row of **T** (each spatial segment) on each distinct component of **C**, along with loadings on the two standard components (constant flat line, Gaussian noise), which are analogous to the intercept and residual error terms in linear regression. $\mathbf{R_2}$ is easily identified using least squares. If too many components are treated as trivial, the RMSE of the Gaussian component will be large, providing a check on the elimination procedure (step 8 in Table 1).

[20] For convenience, before computing $\mathbf{R_2}$ we center **T** (mean = 0 for entire data set) and standardize each time series in **C** (mean = 0, $\sigma = 1$ for each row, and rows multiplied by 1 or −1 to standardize peaking during midday. Here and elsewhere, σ = standard deviation). Standardizing allows responsiveness across different components of **C** to be directly compared by inspection of $\mathbf{R_2}$ (in units of °C of change in **T** per σ of each LDC). Centering **T** gives the constant terms the interpretation of mean temperature anomaly for each spatial segment (i.e., difference between segment mean and reach-wide mean temperature).

[21] In practice, the identification of temperature components is not quite as simple as outlined above, because the computer time involved in finding the initial rotation matrix **R** increases rapidly with the number of rows (number of spatial segments) in **T**. We can expect to identify matrices of 10 or perhaps 20 rows, but the hundreds of rows in a dense data set are not practical. To work around this limit, we preprocess **T** by applying the MI-based clustering algorithm described by *Kraskov et al.* [2005] (step 1 in Table 1). This algorithm arranges the spatial segments into a hierarchical bifurcating tree using mutual information; any number of groups G can be chosen be selecting the corresponding level of the hierarchy, which comprises the least-dependent arrangement of segments into G groups. We then produce a new temperature matrix $\mathbf{T_2}$ with the rows corresponding to the mean time series of each group (step 2 in Table 1), and proceed as described above.

[22] The grouping procedure reduces the number of time series to analyze, while minimizing the loss of information. One can check the adequacy of this reduction at two points further in the analysis: 1) by the occurrence of nearly flat components in the reduced **C**, which shows that the number of groups was sufficient to capture all distinct components; and 2) by small Gaussian noise terms in $\mathbf{R_2}$, which shows the distinct components are sufficient to reconstruct spatial response profiles (sees steps 6 and 8 in Table 1).

3. Application

[23] The method was applied to a 1 km section of Horse Creek, a small intermittent tributary of the Arroyo Seco River near Soledad, California. Horse Creek drains 35.4 km^2 in the interior of the Santa Lucia Mountains, a steeply dissected, rapidly uplifting mountain range in which landslides dominate erosional processes [*Ducea et al.*, 2003]. The Horse Creek catchment receives mean annual rainfall of 67.3 cm, nearly all from October to April, so that summertime flows consist exclusively of a base flow that dwindles over the course of the summer. The catchment is covered mostly in chapparal (dry, fire-prone shrublands) and lies within the Pacific storm track, creating conditions for flashy high flows in the winter that may exceed base flows by three or four orders of magnitude. Air temperatures routinely exceed 35°C in summer.

[24] This creek is typical of many small creeks in the coastal mountains of central and Southern California, where conditions for cold-water biota somehow persist within the hot dry climate [*Boughton et al.*, 2009]. Cold thermal features in this region are thought to depend on some combination of shading by riparian trees; phreatic or hyporheic flows of cold water; and pool volumes that provide thermal buffering [*Boughton et al.*, 2007; *Matthews and Berg*, 1997]. We selected a section of Horse Creek that provided informative contrasts between heavy shade and nearly full sun, between small pools and riffles, and between sections of channel with observable subsurface flow paths versus no observable flow paths (Figure 1).

[25] The informative contrasts occur because the reach straddles a transition between an upstream, perennial, scoured-bedrock channel with dense shade; and a downstream, intermittent, alluvial channel with very sparse shade,

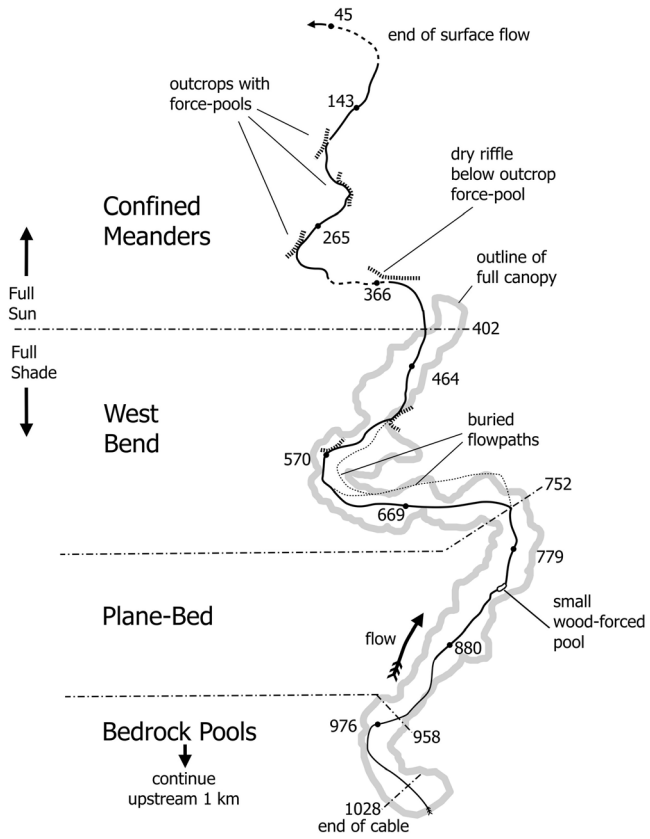

Figure 1. Plan view of the Horse Creek study site (36.249°N, 121.412°W). Numbers are channel positions (meters). Circles mark observation stations with piezometers, air, and bed temperature loggers. DTS cable extended from the end of surface flow upstream to position 1028. Buried flow paths in the West Bend section were inferred from ground-surface form and lines of green herbaceous vegetation.

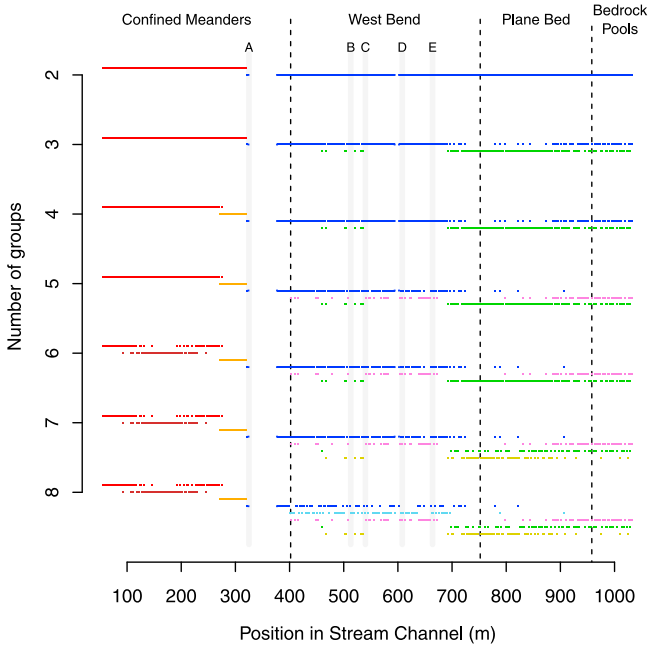

Figure 2. Sequential binary splitting of the study reach into groups of 2 m channel segments using a clustering algorithm based on mutual information. Vertical bands A–E mark locations of hyporheic inputs inferred from channel morphology and riparian vegetation.

about 0.7 km from the confluence at the Arroyo Seco River. The transition had five geomorphically distinct sections (see Tables 2 and S1). The upstream section was the end of a 1 km series of bedrock pools in a sharply confined channel (Figure 1). Pools ranged from 0.5 to 1.5 m deep, interspersed with small bedrock chutes. Directly downstream was a plane bed of disorganized cobbles and small boulders [*Montgomery and Buffington*, 1997] within a narrow, confined valley. Both the bedrock pools and the plane bed were densely shaded by riparian alders (*Alnus sp.*).

[26] Below the plane bed the channel entered a structurally complex "West Bend" area with upper and lower limbs (Figure 1). The upper limb was broad and shallow, confined on the south but opening on the north to a terrace ~70 m wide; attempts to drive piezometers suggested that a sheet of bedrock underlay the channel at 20–30 cm depth. Annual grasses covering the terrace were senescent by May, highlighting a linear depression of green forbs and moist soil, clearly delineating a buried flow path that could be traced to

Table 2. Physical Characteristics of the Horse Creek Study Site

			West Bend		
	Bedrock Pools	Plane Bed	Upper Limb	Lower Limb	Confined Meanders
Discharge (ls^{-1})[a]	18.5	19.9	–	17.4, 18.1	11.6,[b] 17.9, 17.3, 19.0
Gain (% m^{-1})[c]	0.056	0.22	–	0.48, 0.40	0.87,[d] 3.24,[b] −0.082[e]
Mean wetted width (m)	1.9 (0.6)	2.5 (1.0)	3.1 (0.8)	3.0 (1.1)	2.6 (1.2)
Maximum water depth of 2 m segments (quartiles) (cm)	6, 14, 26, 34, 96	6, 12, 14, 18, 80	7, 9, 12, 16, 28	6, 11, 14, 23, 59	1, 8, 11, 14, 52
Gradient (%)	3.5	2.5	1.8	2.6	1.9
Mean middayinsolation (Wm^{-2})	178	241	195	235	630
Piezometer (mean for n = 9 observations/site) (mm)	-	-	-	4 (at 464 m) 1 (at 570 m)	−57 (at 40 m)[f] −34 (at 265 m) −41 (at 366 m)[d]

[a]Salt-tracer method of *Moore* [2004] and an area-under-the-curve estimator. Estimated error is ±2%.
[b]Small estimate from late afternoon, when flows temporarily decline.
[c]Discharge gain per unit channel length, computed from dilution of tracer between two recording sites. Omits losses.
[d]Below versus above dry riffle.
[e]Continuously flowing section downstream of dry riffle. Negative value may be due to evaporation.
[f]Groundwater elevation below dry surface of streambed.

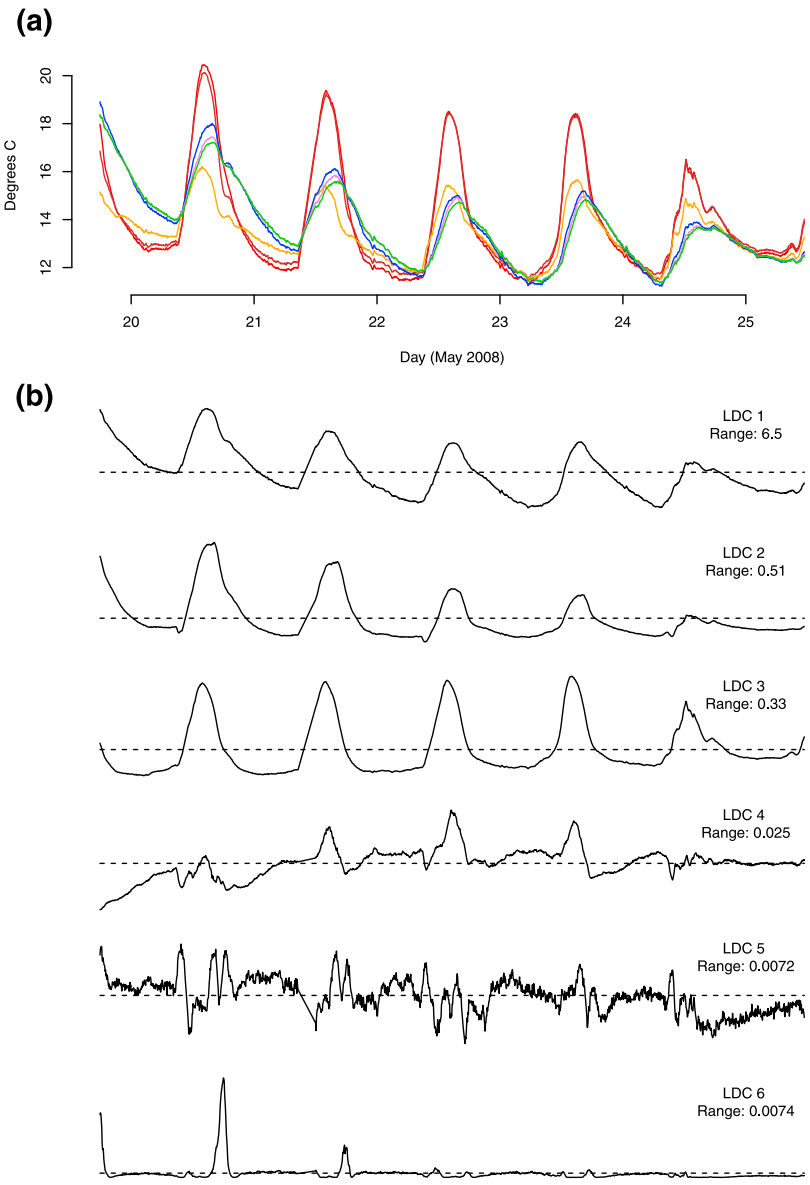

Figure 3. (a) Mean temperatures of segment groups and (b) least-dependent components (LDCs) for DTS time series data divided into six groups. Colors are the same as in Figure 2. Least-dependent components from the MILCA algorithm [*Stogbauer et al.*, 2004] are scaled to sum to the mean temperature series and sorted by amplitude.

its upstream and downstream connections with the channel (see Figure 1). The channel crossed a small rock escarpment at position 664 m to a lower limb (position numbers refer to meter markings on the DTS cable), steeper with a few wood-forced pools and three small bedrock-forced pools. Re-entry of the buried flow paths were discernable at two distinct points and possibly a broader zone. Both limbs were well shaded by alders and oaks (*Alnus*, *Quercus spp.*).

[27] Below position 402 m the valley widened and the channel transitioned to a very sunny series of plane bed riffles interspersed with small bedrock force pools where the meanders encountered the canyon wall. This alluvial section had a dry riffle where daily surface flow disappeared at 375 m and reappeared as a hyporheic seep at 325 m, implying conditions for high heat exchange with the streambed. Surface flow disappeared completely at 69 m. The channel was very sparsely shaded by sycamores (*Platanus racemosa*) (Table 2).

[28] Here we present 5 days of DTS data from early summer 2008. Using a Sensornet Halo DTS, we recorded temperatures each minute at 2 m resolution between midday 19 May 2008 and 25 May 2008, during a week of falling air temperatures. Wind was light except for brief periods of katabatic winds in late afternoon. DTS readings were calibrated with an ice-water bath and a water-temperature logger at cable location 779 m. A malfunction of the power supply created a 3.4 h gap in observations the morning of 21 May; it proved suitable to simply concatenate the data matrices from either side of the gap (creating one Δt equal to 3.4 h in the data set). We removed temperature readings for a dry riffle (location 325 m to 375 m) and a point where the DTS cable

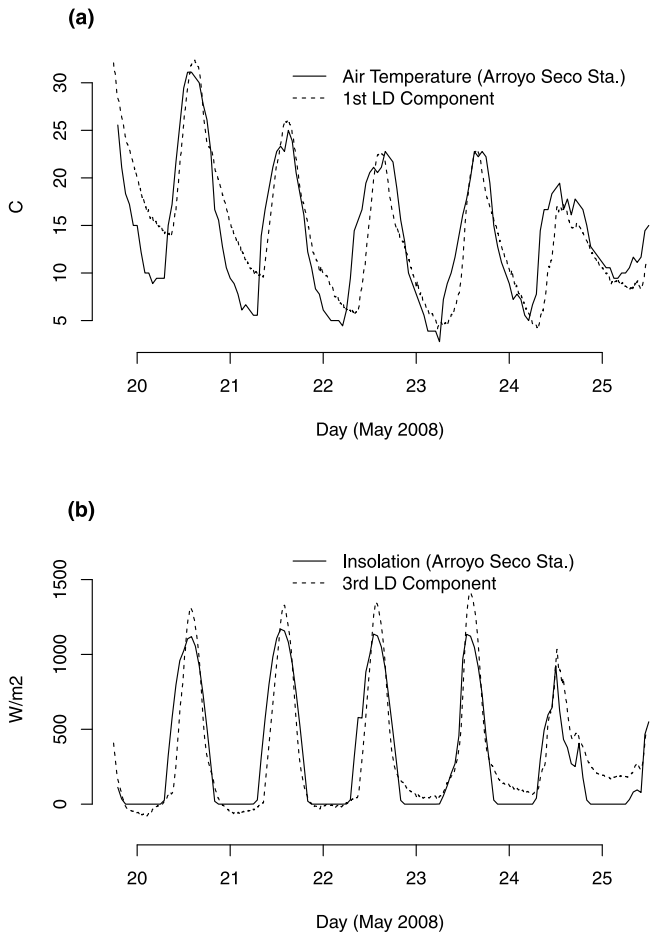

Figure 4. (a) Air temperature and (b) insolation compared to LDC 1 and 3, respectively. Air temperature and insolation data collected at Arroyo Seco Station (36.23°N, 121.49°W).

passed over a log (600 m), because these cable sections were recording temperature of something other than streamflow. The data were then aggregated to 5 min means.

[29] We also logged bed temperature and air temperature at 10 stations spaced throughout the study reach (see Figure 1). Bed temperature was logged with a Hobo Water Temp Pro (accuracy 0.15°C) buried 30–50 cm in the alluvium in midchannel. Air temperature was logged with a Hobo Pendant suspended 1.0 m above the water surface in midchannel (protected by a sunshield). We tracked hydraulic head at 5 stations (45 m, 265 m, 366 m, 464 m and 570 m in Figure 1) using piezometers installed 0.35–0.5 m deep in midchannel (see Table 2) and a weighted, chalk-coated line (accuracy ±1 mm).

3.1. Preprocessing

[30] A plot of MI estimates between pairs of segments revealed substantial structure in the DTS data, with major features that nearly matched the geomorphic sections (see Figure S1 in the auxiliary material[1]). The clustering algorithm showed the greatest distinction of temperature patterns was between the sunny and shady parts of the study reach (number of groups = 2 in Figure 2); the next three splits in the bifurcating tree separated the plane bed segments, the hyporheic seep below the dry riffle, and the bedrock pools from most of the west bend area (number of groups = 3, 4, and 5 in Figure 2). The boundaries identified by MI clustering tended to be displaced downstream 10–20 m relative to geomorphic boundaries identified in the field, which is consistent with a tracer (here heat) becoming well mixed about 10 stream widths downstream (1–5 m wide in the study reach). The fifth split was a discrete section of the confined meanders (number of groups = 6 in Figure 2). Subsequent splits were not as spatially coherent (number of groups = 7 and 8 in Figure 2). We provisionally assumed the 6 group clustering was sufficient to identify all distinct components; this can be checked later by examining RMSE of the $\mathbf{R_2}$ matrix (step 8 in Table 1).

[31] The mean time series for each group illustrates typical temperature patterns (Figure 3a). Not surprisingly, the sunny confined-meander groups showed the highest midday temperatures (red and brown in Figure 3a), except for the hyporheic seep, which tended to exhibit the lowest midday peaks and the highest midnight troughs, especially during the hotter time at the beginning of the observation period (orange in Figure 3a). Partly cloudy conditions on the last full day of observation clearly show up in all groups.

3.2. Distinct Components (LDCs)

[32] LDCA transformed the 6 time series into 6 least-dependent components (LDCs), which were then rescaled as in Table 1 ($\mathbf{C_{mean}}$, steps 3 to 5) and sorted by amplitude (range) (step 6). The sorting arranges the LDCs in order of decreasing contribution to the mean time series (mean temperature series for all spatial segments).

[33] LDC 1 had the largest amplitude: range = 6.5°C (Figure 3b, first row). Daily fluctuations were asymmetric, trailing off each afternoon and night, followed by an abrupt rise each daybreak and a peak each early afternoon; there was also a multiday cooling trend. Superimposing LDC 1 and hourly weather data from Arroyo Seco Station (6 km west) showed a remarkable similarity in shape (Figure 4a; LDC 1 rescaled to mean and σ of station data). Differences were the slightly earlier morning climb of LDC 1 (consistent with different topographic shading at study site versus weather station), and a steeper decline in daily minimum temperatures relative to daily maximums. A regression showed that LDC 1 closely covaried with hourly air temperature, but also somewhat with insolation data from the same weather station (Table 3). Overall, LDC 1 appears to involve heat fluxes that are primarily coordinated with fluctuations in air temperature.

Table 3. Best Fitting Regression of Standardized Components on Nearest Weather Station Data[a]

Component	Regression Coefficients		Nash-Sutcliffe Model Fit
	Air Temperature	Insolation	
LDC 1	1.04	−0.24	0.73
LDC 2	0.84	–	0.70
LDC 3	–	0.92	0.85
LDC 4	−1.07	1.28	0.58
LDC 5	–	–	0.01
LDC 6	−0.32	0.23	0.04

[a]Dependent and independent variables standardized (mean = 0, SD = 1); best fitting model selected using AIC; candidate models were all combinations of 0, 1, or 2 covariates.

[1]Auxiliary materials are available in the HTML. doi:10.1029/2011WR011713.

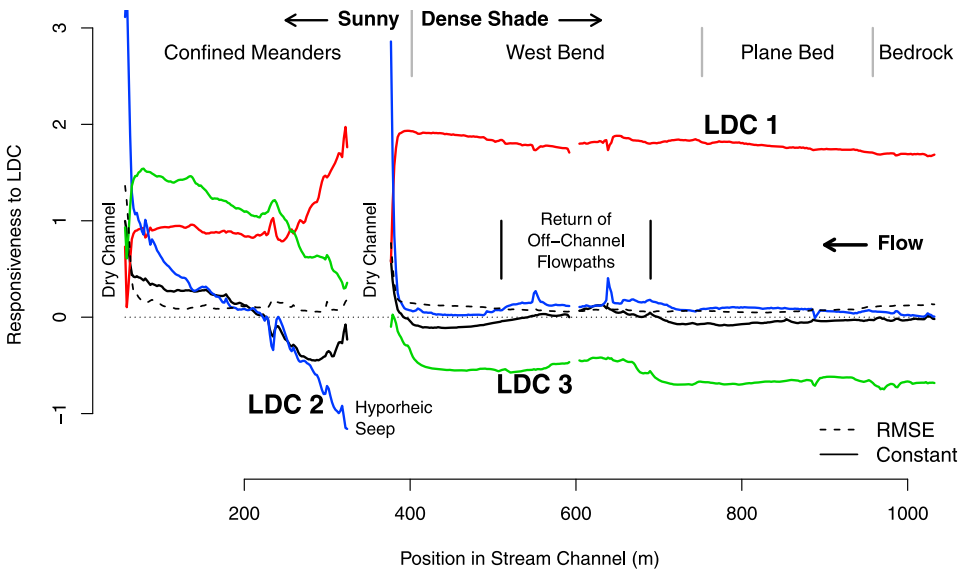

Figure 5. Spatial response profiles for 2 m stream segments and LDCs 1 through 3. The y axis gives °C/σ for LDCs and °C for the constant and RMSE terms.

[34] LDC 2 had a shape generally similar to LDC 1 and air temperature, but relative amplitude compared to LDC 1 was only 8% (range = 0.51°C versus 6.5°C), peaks occurred slightly later in the day, nighttime declines were more gradual, and nightly minimums were more stable (Figure 3b, second row versus first row). Regression showed an association with air temperature, though weaker than that of LDC 1 (Table 3). LDC 2's strongest loading in rotation matrix **R** was a negative association with the hyporheic seep below the dry riffle (i.e., the orange group in Figure 2), suggesting a relation to subsurface flows and the streambed. Overall, LDC 2 had a similar, but more refractory, shape compared to LDC 1.

[35] LDC 3 displayed a symmetric half-sine wave pattern, centered on solar noon and bracketed by sunrise and sunset (Figure 3b, third row). This is remarkably close to local insolation patterns, including the spiky profile on the partly cloudy day of 24 May (Figure 4b). The match is confirmed by simple regression (Table 3). The major discrepancy was a moderate trend in nightly minimums. Like LDC 1, LDC 3 had a delayed morning rise relative to the weather station data, again suggesting differences in topographic shading. Relative amplitude of LDC 2 was 5% (0.33°C versus 6.5°C for LDC 1).

[36] LDCs 4 through 6 had very small ranges (0.4% to 0.1% amplitude relative to LDC 1). For clarity, Figure 3b shows standardized versions of all six components, but if scaled proportionately the last three components would appear virtually flat. We conclude they are trivial components, and replace them with the two standard components (flat line, Gaussian noise; step 6 in Table 1). This decision can be checked later by ensuring that the Gaussian noise terms (root-mean-squared error, or RMSE) are acceptably small in spatial response profiles (step 8 in Table 1; see section 3.3).

3.3. Spatial Response Profiles

[37] The final $\mathbf{R_2}$ matrix was computed from standardized LDCs ($\mathbf{C_z}$, steps 7 and 8 in Table 1), which facilitates comparisons of spatial response profiles. Each column of $\mathbf{R_2}$ represents a spatial response profile for a particular LDC, in units of temperature change in the spatial segments (unit: °C) per standardized change in the LDC (unit: σ). For example, a value of 2 indicates that water temperature at a segment increases +2°C per change of +1σ in an LDC (positive response), whereas a value of −1 indicates water temperature at the segment cools by −1°C per change of +1σ in an LDC (negative response). Values close to zero imply temperature patterns at a segment are nearly independent of the LDC. Due to the standardization, comparisons can be made in the responsiveness of different spatial segments to the same LDC (spatial response), or of one segment to different LDCs (relative response).

[38] Spatial profiles for the two standard components (flat line, RMSE) have slightly different interpretations. The column of $\mathbf{R_2}$ corresponding to the flat line represents spatial anomalies, defined as the mean temperature of a segment relative to mean temperature of all segments (unit: °C). The column of $\mathbf{R_2}$ corresponding to RMSE (Gaussian noise) is the residual error of **T** after the spatial anomalies and responsiveness of LDCs are taken into account (unit: °C). It shows how much information was lost by grouping the time series initially (steps 1 and 2 in Table 1) and by treating nearly flat components as trivial (step 6 in Table 1).

[39] Below we present spatial response profiles for water temperatures from the DTS (Figure 5), and also for the air and bed temperatures at the 10 stations with data loggers (Figure 6). For water, the spatial profile for RMSE (dashed line in Figure 5) was only ∼0.1°C for most of its length, suggesting that grouping the data and eliminating trivial LDCs did not discard significant pattern. Notable exceptions were two points just upstream of dry sections (375 m and 69 m), where RMSE jumped to ∼1°C.

[40] LDC 1, whose temporal pattern matched air temperature, had a spatial response profile that was highly positive in the upstream shaded section (400 m to 1050 m; Figure 5, red), with stream temperature changing nearly +2°C per σ of LDC 1. Downstream in the sunny section the responsiveness steeply declined by about 50% but then leveled out—suggestive of a transition to a weaker but

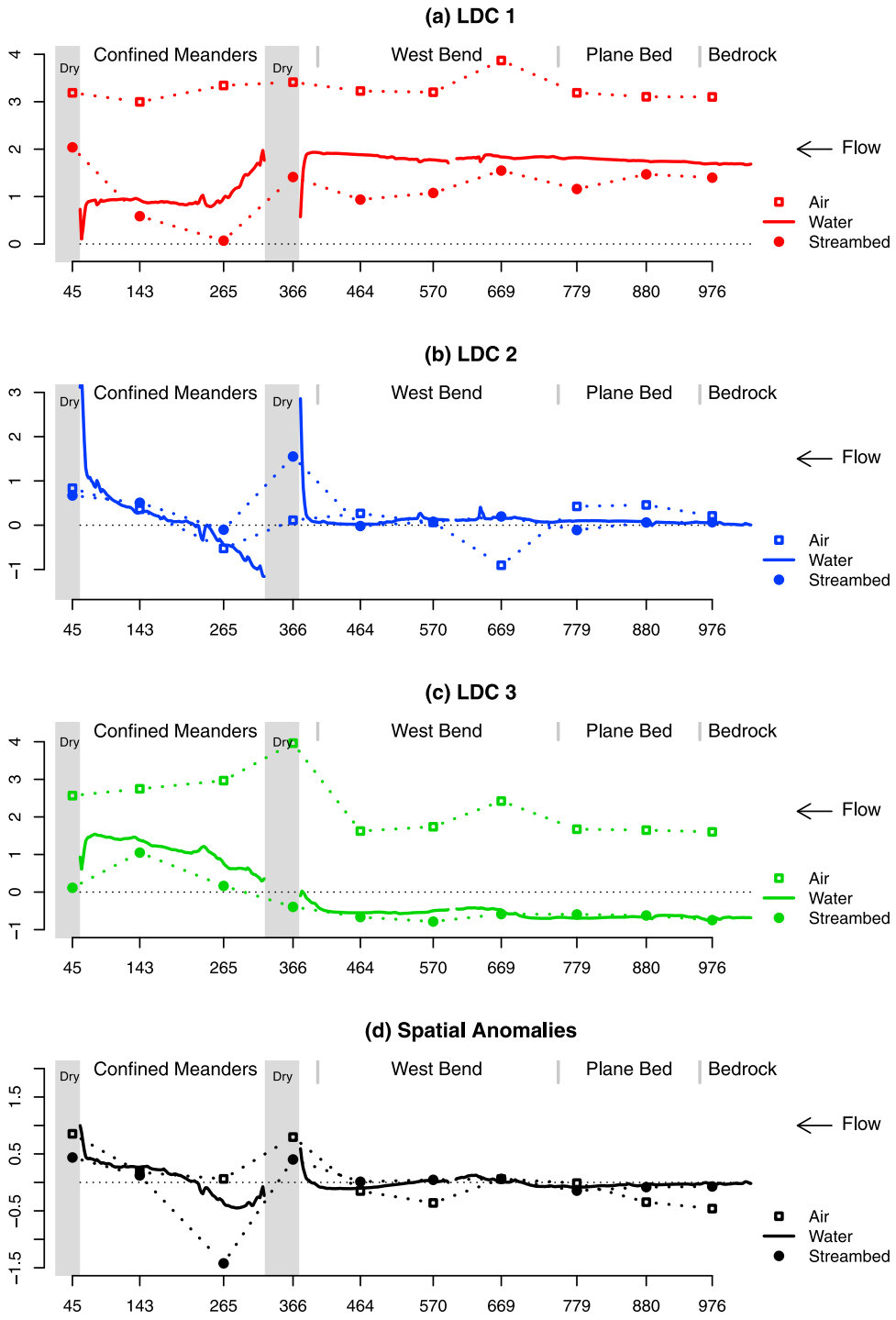

Figure 6. Spatial response profiles ($\mathbf{R_2}$ matrix) for ten stations measuring streambed and air temperatures 0.35–0.5 m below and 1.0 m above the thalweg, respectively. Stations at 45 and 366 m were in sections of channel with no consistent surface flow.

stable relationship between stream temperature and air temperature in the sunny section. The response of the air loggers suspended above the stream was similar but even stronger; and the bed loggers, (mostly) weaker (Figure 6a). This is consistent with LDC 1 being related to fluctuations in aboveground conditions such as air temperature.

[41] The spatial profile for LDC 2 was quite negative just below the dry riffle (Figure 5, blue), indicating a midday heat subtraction of about −1.2°C per σ of LDC 2 at the point where surface flow reappears. This is consistent with LDC 2 being a signature of heat absorption by subsurface processes. Immediately downstream the profile rapidly climbed to zero and then into positive territory, implying a downstream reversal of heat subtraction to heat addition during midday (see Figure S2 in the auxiliary material). This interpretation is corroborated by bed temperatures in the confined meanders (See stations at positions 45 through 366 in Figure 6b). The bed responses were stronger (more positive) than air and

water responses at the wet stations (143 and 265), and especially strong at one dry stations (366), suggesting a tighter link of LDC 2 to subsurface heat fluxes than to aboveground fluxes.

[42] Upstream in the shady section the water's response profile was generally quite close to zero (i.e., nearly independent of LDC 2), except at two notable rounded humps between 700 m and 500 m (Figure 5, blue). These humps imply a modest heating response for LDC 2, and were near points where buried flow paths reconnected to the channel (two other, sharp peaks are artifacts of small bits of cable lying on dry bed during afternoon low flows).

[43] Somewhat surprisingly, LDC 3 had a spatial profile that was consistently negative in the shady section (Figure 5, green), suggesting heat subtraction on the order at least $-0.5°C$ to $-0.7°C/\sigma$, corresponding to a midday temperature reduction of at least 2.0–2.2°C on sunny days. Since LDC 3 appears to be closely associated with daily insolation (see Figure 4b and Table 3), this suggests dense shading does not just make the water temperature independent of insolation, but in fact negatively responsive to it. This relationship did not hold for air temperature 1 m above the water's surface, which showed a consistent, strong, positive response to LDC 3 (Figure 6c).

[44] Downstream in the sunny section the profile for LDC 3 climbed steeply (Figure 5, green), rapidly exceeding the profile of LDC 1 and maintaining a response at least $+1°C/\sigma$ in most of the confined meander. This suggests strong addition of heat whose time evolution closely tracks solar insolation, and indicates opposite thermal responses to LDC 3 in the shaded and unshaded sections (see Figure S3 in auxiliary material). In the sunny section the bed temperatures were less responsive and the air temperatures more responsive than the water temperatures (Figure 6c). This is consistent with a link between LDC 3 and aboveground heat fluxes.

[45] The spatial anomalies (Figure 5, black) show mean temperature for each 2 m segment relative to mean temperature for the entire study reach, and confirmed that the most heated segments were at the bottom of the sunny section and the most cooled segments were directly downstream of the dry riffle. Despite the dry riffle's very sunny position, bed temperature below the riffle was much cooler than anywhere else and much cooler than the surface water (Figure 6d). In the shady segments upstream, the water was buffered to stay within $\pm 0.2°C$ of the reach-wide mean. Here, bed temperature tended to match water temperature, but the air temperature 1 m above the water was often cooler than the water (Figure 6d).

[46] To ask if all three components were necessary to reconstruct spatial profiles, we re-estimated $\mathbf{R_2}$ three more times, each time omitting one of the LDCs. The fit of these reduced linear combinations was vastly poorer as judged by Akaike's Information Criterion [*Burnham and Anderson*, 2001] (typically AICs larger by 1000–5000), except for LDC 2 in three small areas where its response profile was close to zero. This confirmed that important information is lost if any of the three LDCs were omitted.

4. Discussion

[47] We found at least three distinct components were necessary to explain temperature patterns in this transitional section of Horse Creek, achieving RMSE $\sim 0.1°C$ everywhere except two locations right where surface flow was disappearing (presumably some combination of evaporation and infiltration). The direction and relative magnitude of air versus water versus bed responses in the spatial profiles suggested that the first and third components were more closely related to aboveground heat fluxes than subsurface heat fluxes. Both formal inference and visual inspection of the components' time evolution suggested that the first component was proportionate to air temperature and the third component proportionate to insolation, two meteorological forcings commonly found to dominate heat budgets [*Gu and Li*, 2002; *Sinokrot and Stefan*, 1994]. The second component had a more complicated pattern suggesting a refractory tracking of air temperature and linkage to subsurface heat fluxes, at least in some parts of the study reach.

[48] The study reach had three general contrasts: small pools versus riffles, shady versus sunny, and observable subsurface flow paths versus no subsurface flow paths. We observed no obvious differences in spatial profiles between pools and riffles (e.g., between the bedrock and plane bed sections in Figure 5). However, the shady and sunny sections were quite different. In the shady section the first distinct component (LDC 1) clearly dominated temperature dynamics (Figure 5, right); in the sunny section the first and third components (LDC 1, LDC 3) had roughly comparable contributions (Figure 5, left). This is consistent with heat fluxes mostly proportionate to air temperature in shady reaches, but a combination of heat fluxes proportionate to air temperature and insolation in sunny reaches. If one wanted to measure the individual heat flux elements making up the two components, the relative flatness of the spatial profiles in the shady section (Figure 5, right) suggests that results will not be too terribly sensitive to the exact location chosen to make the measurements. This is not the case for the sunny section, especially for LDC 3 which climbs quite steeply, implying no one location is representative.

4.1. A Component Negatively Proportionate to Insolation

[49] Inference suggested that LDC 3 was composed of heat flux elements that vary proportionate with insolation patterns. It is therefore curious to note the negative spatial profile of LDC 3 in the shady section (Figure 5, green). If the effect of vegetation were purely to shade out insolation (long- and short-wave radiation), then the shady reach should decouple from insolation patterns, meaning LDC 3 should be close to zero or perhaps weakly positive. The fact that it is negative suggests a subtraction of heat from the channel water proportionate to the level of insolation. One possible mode of heat subtraction might be heat movement into the bed—for example via hyporheic flows [*Acuna and Tockner*, 2009; *Burkholder et al.*, 2008]—but one would need to propose a mechanism by which such heat movement stays so closely proportionate to insolation. It is also possible that evapotranspiration of the riparian canopy provides a plausible mechanism for heat subtraction upward, because evapotranspiration tends to produce gradients between leaf surface temperature and ambient air temperature [*Alexandridis et al.*, 2009]. This could set up a net movement of sensible heat and/or long-wave radiation from the water to the canopy that should stay fairly proportionate to insolation.

[50] In most of the shaded section the mean air temperature 1 m above the water is slightly cooler than the water itself (Figure 6d), indicating some amount of upward conduction of sensible heat. If sensible heat conduction were the primary flux than the air temperatures should have an even stronger negative association with LDC 3 than the water, but we observed the opposite, a strong positive response (Figure 6c), suggesting that long-wave radiation more likely dominates. Since the energy content of long-wave radiation emitted by a water or vegetation surface is proportional to its absolute temperature (°K) raised to the fourth power [*Bogan et al.*, 2003; *Mohseni and Stefan*, 1999], long-wave energy flow could be quite responsive to differences in temperature between the canopy and channel-water surfaces. This is consistent with findings of *Benyahya et al.* [2012], where long-wave radiative flux between a small creek and a fully closed tree canopy was 10 times greater than sensible heat flux, and much more responsive to changes in canopy cover during spring leafing-out.

[51] In their data however, net long-wave radiation with the canopy did not subtract heat from the water; it simply added it more slowly than solar short-wave radiation would have added heat if not intercepted by the canopy. Their site was in humid temperate forest; the riparian trees of Horse Creek occur in a hot arid landscape but are themselves not water limited during the dry season. Perhaps the contrast of hot dry air and unlimited evapotranspiration in full sunlight allows riparian trees to set up sufficiently cool leaf surfaces to sustain net absorption of long-wave radiation from the water below. This hypothesis would testable by combining standard element-wise heat budget methods with the distinct-components approach used here, and raises the interesting possibility that peak temperatures of small shaded creeks may to some degree be under biological control.

4.2. A Complex, Refractory Component

[52] Inference suggested that LDC 2 was composed of heat flux elements that tracked air temperature, but more weakly and with greater delays than LDC 1. LDC 2 had a complex spatial profile. Its strongest responses were two sharp upward peaks at the two points where surface flows were going subsurface; its next strongest response was a sharp negative spike at the hyporheic seep just below the dry riffle, attenuating with distance downstream (Figure 5, blue). The next most notable features of the spatial profile (disregarding two small spikes thought to be artifacts of DTS cable exposure) were two small positive humps that broadly overlapped the zone where off-channel buried flow paths were observed to return to the stream (between positions 520 m and 680 m). All these observations are consistent with LDC 2 being involved in subsurface heat exchanges that evolve similarly to air temperatures, but with a more gradual response than air temperatures and with more stable nightly minimums.

[53] Only below the hyporheic seep was this refractory component associated with a cooling (negative) response of streamflow. The returns of the off-channel flow paths in the shady section were associated with small heating responses of the stream, suggesting that incoming water was warmer than streamflow at midday. We note that these off-channel flow paths, discernable in the terrace via slight depressions and differences in ground vegetation, were mostly outside the immediate riparian zone where dense shading occurred. They mostly ran through hot, sunny oak savanna adjacent to the riparian corridor, and so could easily be accumulating heat before returning water to the stream. At both the top and bottom of the sunny section, the heating response of streamflow was even greater. Streamflow here was confined to a narrow band within a wider dry bed of cobbles and gravel fully exposed to sun and air. One possible mechanism is that the dry bed heats sufficiently to drive substantial lateral conduction of heat into the streamflow, which of course has been advected from cooler conditions upstream. In the sunny section this pattern of heat conduction would tend to produce a more positive response to LDC 2 by bed temperatures than by water temperatures, and an especially strong response by bed temperatures in the dry sections of channel. This pattern can be observed on the left side of Figure 6b.

[54] By contrast, subsurface heat fluxes are generally expected to be accepting heat during spring and early summer, because the weather heats faster than the ground (and groundwater), with streamflows somewhere in between [*Bogan et al.*, 2003, 2004]. The refractory component described here suggests a more complicated picture, possibly due to shallow lateral movements of stored heat in the ground of riparian corridors with complex shading patterns [see also *Westhoff et al.*, 2011]. This general hypothesis would be testable using element-wise heat budget methods that include temperature sensors recording shallow ground temperatures. We note here, however, that in our study area the spatial profile of the refractory component ranged from strongly negative to near zero to strongly positive. This suggests that results from element-wise heat budgets would be very sensitive to the location of sensors. It may often prove useful to first generate a component-wise heat budget that includes spatial profiles such as Figure 5, to provide context to element-wise study designs.

4.3. Conclusions

[55] For a small section of arid-land creek, the method of distinct components allowed us to identify three distinct signals in dense temperature data, none of which could be eliminated without losing important information about thermal heterogeneity. We conclude that the heat budget of the creek had three general components, each probably consisting of multiple heat flux elements with coordinated dynamics. Formal and informal inference about the shape (time evolution) of the components allowed us to link two components to meteorological forcings, and propose an interpretation of the third as reflecting both a meteorological forcing and refractory subsurface heat fluxes. By comparing spatial response profiles for each component to structural heterogeneity at the creek site (pools versus riffles, shaded versus sunny, occurrence of subsurface flow paths), we were able generate two new and testable hypotheses about process heterogeneity. The first hypothesis is that dense riparian canopies may remove substantial heat from arid-land streams via exchange of long-wave radiation. The second is that lateral subsurface movement of heat may be an important contributor of heat to arid-land streams.

[56] The method does not resolve individual heat flux elements, so process inference from the method will generally have the status of hypotheses needing further testing by conventional element-wise heat budgets. At the same time, the method provides finer spatial resolution than element-wise heat budgets, and thus can provide landscape context

for the more detailed element-wise methods that typically focus on a particular point in a stream. Element-wise budgets involve an implicit assumption that heat flux elements measured at a small number of points are representative of the broader riparian system, and the component-wise method outlined here can be used to evaluate this hypothesis. For example, we found that in the shady section of our study reach the components had relatively flat spatial profiles, suggesting that detailed heat flux measurements at any one point would be broadly representative. However, in the sunny section, spatial profiles for two of the components were steeply inclined, and one component was associated with daytime warming in some areas and daytime cooling in others, suggesting that conclusions from an element-wise heat budget will be very sensitive to placement of sensors. But the profiles also suggest where one might place sensors to measure minimum or maximum affect of a particular component. Thus the element-wise and component-wise methods can provide complementary insights to the same study area.

[57] Our experience with the method in this study suggests it will be useful for generating new hypotheses; for selecting informative sites for detailed element-wise methods; for determining the dimensionality of heat budgets (number of distinct components) in natural streams, and more broadly for associating thermal components to fluvial structure and processes.

[58] **Acknowledgments.** We thank Cameron Chabre and the Big Sur Land Trust for providing access to the study site. Appreciation goes also to Barry Freifeld for loaning us the DTS and to Dave Rundio, Steve Lindley, Heidi Fish, Matt Jones, Tommy Williams, and Eric Danner for help deploying the fiber-optic cable. Andrew Pike provided many useful insights during a series of discussions that greatly improved the work. Steve Lindley, Eric Danner, Ted Endreny, Michael L. Roderick, and one anonymous reviewer commented quite helpfully on the manuscript.

References

Acuna, V., and K. Tockner (2009), Surface-subsurface water exchange rates along alluvial river reaches control the thermal patterns in an Alpine river network, *Freshwater Biol.*, *54*, 306–320, doi:10.1111/j.1365-2427.2008.02109.x.

Alexandridis, T. K., I. Cherif, Y. Chemin, G. N. Silleos, E. Stavrinos, and G. C. Zalidis (2009), Integrated methodology for estimating water use in Mediterranean agricultural areas, *Remote Sens.*, *1*, 445–465, doi:10.3390/rs1030445.

Arrigoni, A. S., G. C. Poole, L. A. K. Mertes, S. J. O'Daniel, W. W. Woessner, and S. A. Thomas (2008), Buffered, lagged, or cooled? Disentangling hyporheic influences on temperature cycles in stream channels, *Water Resour. Res.*, *44*, W09418, doi:10.1029/2007WR006480.

Benyahya, L., D. Caissie, M. G. Satish, and N. El-Jabi (2012), Long-wave radiation and heat flux estimates within a small tributary in Catamaran Brook (New Brunswick, Canada), *Hydrol. Processes*, *26*, 475–484, doi:10.1002/hyp.8141.

Bogan, T., O. Mohseni, and H. G. Stefan (2003), Stream temperature-equilibrium temperature relationship, *Water Resour. Res.*, *39*(9), 1245, doi:10.1029/2003WR002034.

Bogan, T., H. G. Stefan, and O. Mohseni (2004), Imprints of secondary heat sources on the stream temperature/equilibrium temperature relationship, *Water Resour. Res.*, *40*, W12510, doi:10.1029/2003WR002733.

Boughton, D. A., M. Gibson, R. Yedor, and E. Kelley (2007), Stream temperature and the potential growth and survival of juvenile *Oncorhynchus mykiss* in a Southern California creek, *Freshwater Biol.*, *52*, 1353–1364, doi:10.1111/j.1365-2427.2007.01772.x.

Boughton, D. A., H. Fish, J. Pope, and G. Holt (2009), Spatial patterning of habitat for *Oncorhynchus mykiss* in a system of intermittent and perennial streams, *Ecol. Freshwater Fish*, *18*, 92–105, doi:10.1111/j.1600-0633.2008.00328.x.

Boyd, M., and B. Kasper (2003), *Analytical Methods for Dynamic Open Channel Heat and Mass Transfer: Methodology for Heat Source Model Version 7.0*, Oregon Dep. of Environ. Quality, Portland, Ore.

Brown, G. W. (1969), Predicting temperatures of small streams, *Water Resour. Res.*, *5*, 68–75, doi:10.1029/WR005i001p00068.

Burkholder, B. K., G. E. Grant, R. Haggerty, T. Khangaonkar, and P. J. Wampler (2008), Influence of hyporheic flow and geomorphology on temperature of a large, gravel-bed river, Clackamas River, Oregon, USA, *Hydrol. Processes*, *22*, 941–953, doi:10.1002/hyp.6984.

Burnham, K. P., and D. R. Anderson (2001), Kullback–Leibler information as a basis for strong inference in ecological studies, *Wildlife Res.*, *28*, 111–119, doi:10.1071/WR99107.

Caissie, D. (2006), The thermal regime of rivers: A review, *Freshwater Biol.*, *51*, 1389–1406, doi:10.1111/j.1365-2427.2006.01597.x.

Caissie, D., N. El-Jabi, and M. G. Satish (2001), Modelling of maximum daily water temperatures in a small stream using air temperatures, *J. Hydrol.*, *251*, 14–28, doi:10.1016/S0022-1694(01)00427-9.

Ducea, M., M. A. House, and S. Kidder (2003), Late Cenozoic denudation and uplift rates in the Santa Lucia Mountains, *Calif. Geol.*, *31*, 139–142.

Eaton, J. G., and R. M. Scheller (1996), Effects of climate warming on fish thermal habitat in streams of the United States, *Limnol. Oceanogr.*, *41*, 1109–1115, doi:10.4319/lo.1996.41.5.1109.

Ebersole, J. L., W. J. Liss, and C. A. Frissell (2001), Relationship between stream temperature, thermal refugia and rainbow trout *Oncorhynchus mykiss* abundance in arid-land streams in the northwestern United States, *Ecol. Freshwater Fish*, *10*, 1–10, doi:10.1034/j.1600-0633.2001.100101.x.

Ebersole, J. L., W. J. Liss, and C. A. Frissell (2003), Thermal heterogeneity, stream channel morphology, and salmonid abundance in northeastern Oregon streams, *Can. J. Fish. Aquat. Sci.*, *60*, 1266–1280, doi:10.1139/f03-107.

Evans, E. C., G. R. McGregor, and G. E. Petts (1998), River energy budgets with special reference to river bed processes, *Hydrol. Processes*, *12*, 575–595, doi:10.1002/(SICI)1099-1085(19980330)12:4<575::AID-HYP595>3.0.CO;2-Y.

Gu, R. R., and Y. T. Li (2002), River temperature sensitivity to hydraulic and meteorological parameters, *J. Environ. Manage.*, *66*, 43–56, doi:10.1006/jema.2002.0565.

Hannah, D. M., I. A. Malcolm, C. Soulsby, and A. F. Youngson (2008), A comparison of forest and moorland stream microclimate, heat exchanges and thermal dynamics, *Hydrol. Processes*, *22*, 919–940, doi:10.1002/hyp.7003.

Hebert, C., D. Caissie, M. G. Satish, and N. El-Jabi (2011), Study of stream temperature dynamics and corresponding heat fluxes within Miramichi River catchments (New Brunswick, Canada), *Hydrol. Processes*, *25*, 2439–2455, doi:10.1002/hyp.8021.

Isaak, D. J., and W. A. Hubert (2004), Nonlinear response of trout abundance to summer stream temperatures across a thermally diverse montane landscape, *Trans. Am. Fish. Soc.*, *133*, 1254–1259, doi:10.1577/T03-010.1.

Isaak, D. J., C. H. Luce, B. E. Rieman, D. E. Nagel, E. E. Peterson, D. L. Horan, S. Parkes, and G. L. Chandler (2010), Effects of climate change and wildfire on stream temperatures and salmonid thermal habitat in a mountain river network, *Ecol. Appl.*, *20*, 1350–1371, doi:10.1890/09-0822.1.

Johnson, S. L. (2004), Factors influencing stream temperatures in small streams: Substrate effects and a shading experiment, *Can. J. Fish. Aquat. Sci.*, *61*, 913–923, doi:10.1139/f04-040.

Kraskov, A., H. Stogbauer, and P. Grassberger (2004), Estimating mutual information, *Phys. Rev. E*, *69*, 066138, doi:10.1103/PhysRevE.69.06613. [Erratum, *Phys. Rev. E*, 83, 019903(E), doi:10.1103/PhysRevE.83.019903, 2001.], doi:10.1103/PhysRevE.69.066138.

Kraskov, A., H. Stogbauer, R. G. Andrzejak, and P. Grassberger (2005), Hierarchical clustering using mutual information, *Europhys. Lett.*, *70*, 278–284, doi:10.1209/epl/i2004-10483-y.

Leach, J. A., and R. D. Moore (2010), Above-stream microclimate and stream surface energy exchanges in a wildfire-disturbed riparian zone, *Hydrol. Processes*, *24*, 2369–2381.

Mantua, N., I. Tohver, and A. Hamlet (2010), Climate change impacts on streamflow extremes and summertime stream temperature and their possible consequences for freshwater salmon habitat in Washington State, *Clim. Change*, *102*, 187–223, doi:10.1007/s10584-010-9845-2.

Matthews, K. R., and N. H. Berg (1997), Rainbow trout responses to water temperature and dissolved oxygen stress in two Southern California stream pools, *J. Fish Biol.*, *50*, 50–67, doi:10.1111/j.1095-8649.1997.tb01339.x.

Matthews, K. R., N. H. Berg, D. L. Azuma, and T. R. Lambert (1994), Cool water formation and trout habitat use in a deep pool in the Sierra Nevada,

California, *Trans. Am. Fish. Soc.*, *123*, 549–564, doi:10.1577/1548-8659(1994)123<0549:CWFATH>2.3.CO;2.

Mohseni, O., and H. G. Stefan (1999), Stream temperature air temperature relationship: A physical interpretation, *J. Hydrol.*, *218*, 128–141, doi:10.1016/S0022-1694(99)00034-7.

Mohseni, O., H. G. Stefan, and T. R. S. T. E. Erickson (1998), A nonlinear regression model for weekly stream temperatures, *Water Resour. Res.*, *34*, 2685–2692, doi:10.1029/98WR01877.

Mohseni, O., H. G. Stefan, and J. G. Eaton (2003), Global warming and potential changes in fish habitat in US streams, *Clim. Change*, *59*, 389–409, doi:10.1023/A:1024847723344.

Montgomery, D. R., and J. M. Buffington (1997), Channel-reach morphology in mountain drainage basins, *Geol. Soc. Am. Bull.*, *109*, 596–611, doi:10.1130/0016-7606(1997)109<0596:CRMIMD>2.3.CO;2.

Moore, R. D. (2004), Introduction to salt dilution gauging for streamflow measurement. Part 2: Constant-rate injection, *Streamline Watershed Manage. Bull.*, *8*(1), 11–15.

Morrill, J. C., R. C. Bales, and M. H. Conklin (2005), Estimating stream temperature from air temperature: Implications for future water quality, *J. Environ. Eng.*, *131*, 139–146, doi:10.1061/(ASCE)0733-9372(2005)131:1(139).

Ormerod, S. J. (2009), Climate change, river conservation and the adaptation challenge, *Aquat. Conserv. Mar. Freshwater Ecosyst.*, *19*, 609–613, doi:10.1002/aqc.1062.

Poff, N. L., et al. (2010), The ecological limits of hydrologic alteration (ELOHA): A new framework for developing regional environmental flow standards, *Freshwater Biol.*, *55*, 147–170, doi:10.1111/j.1365-2427.2009.02204.x.

Poole, G. C., and C. H. Berman (2001), An ecological perspective on in-stream temperature: Natural heat dynamics and mechanisms of human-caused thermal degradation, *Environ. Manage. N. Y.*, *27*, 787–802, doi:10.1007/s002670010188.

Shannon, C. E. (1948), A mathematical theory of communication, *Bell Syst. Tech. J.*, *27*, 379–423, 623–656.

Sinokrot, B. A., and H. G. Stefan (1994), Stream water-temperature sensitivity to weather and bed parameters, *J. Hydraul. Eng.*, *120*, 722–736, doi:10.1061/(ASCE)0733-9429(1994)120:6(722).

Stogbauer, H., A. Kraskov, S. A. Astakhov, and P. Grassberger (2004), Least-dependent-component analysis based on mutual information, *Phys. Rev. E*, *70*, 066123, doi:10.1103/PhysRevE.70.066123, doi:10.1103/PhysRevE.70.066123.

Story, A., R. D. Moore, and J. S. Macdonald (2003), Stream temperatures in two shaded reaches below cutblocks and logging roads: Downstream cooling linked to subsurface hydrology, *Can. J. For. Res.*, *33*, 1383–1396, doi:10.1139/x03-087.

Thorp, J. H., M. C. Thoms, and M. D. Delong (2006), The riverine ecosystem synthesis: Biocomplexity in river networks across space and time, *River Res. Appl.*, *22*, 123–147, doi:10.1002/rra.901.

Torgersen, C. E., D. M. Price, H. W. Li, and B. A. McIntosh (1999), Multiscale thermal refugia and stream habitat associations of chinook salmon in northeastern Oregon, *Ecol. Appl.*, *9*, 301–319, doi:10.1890/1051-0761(1999)009[0301:MTRASH]2.0.CO;2.

Webb, B. W., and Y. Zhang (1997), Spatial and seasonal variability in the components of the river heat budget, *Hydrol. Processes*, *11*, 79–101, doi:10.1002/(SICI)1099-1085(199701)11:1<79::AID-HYP404>3.0.CO;2-N.

Webb, B. W., and Y. Zhang (2004), Intra-annual variability in the non-advective heat energy budget of Devon streams and rivers, *Hydrol. Processes*, *18*, 2117–2146, doi:10.1002/hyp.1463.

Webb, B. W., D. M. Hannah, R. D. Moore, L. E. Brown, and F. Nobilis (2008), Recent advances in stream and river temperature research, *Hydrol. Processes*, *22*, 902–918, doi:10.1002/hyp.6994.

Westhoff, M. C., M. N. Gooseff, T. A. Bogaard, and H. H. G. Savenije (2011), Quantifying hyporheic exchange at high spatial resolution using natural temperature variations along a first-order stream, *Water Resour. Res.*, *47*, W10508, doi:10.1029/2010WR009767.

Wilby, R. L., et al. (2010), Evidence needed to manage freshwater ecosystems in a changing climate: Turning adaptation principles into practice, *Sci. Total Environ.*, *408*, 4150–4164, doi:10.1016/j.scitotenv.2010.05.014.